BIOLOGY OF REPRODUCTION (2013) **88**(2):76, 1–11
Published online before print 26 December 2012.
DOI 10.1095/biolreprod.111.098673

Meiosis I Arrest Abnormalities Lead to Severe Oligozoospermia in Meiosis 1 Arresting Protein (*M1ap*)-Deficient Mice[1]

Nelson Alexander Arango,[2,3,4] Li Li,[3,5] Deepa Dabir,[6] Fotini Nicolau,[4] Rafael Pieretti-Vanmarcke,[4] Carla Koehler,[7] John R. McCarrey,[8] Naifang Lu,[9] and Patricia K. Donahoe[4]

[4]*Pediatric Surgical Research Laboratories, Massachusetts General Hospital and Harvard Medical School, Boston, Massachusetts*
[5]*Department of Molecular Biology, Massachusetts General Hospital and Harvard Medical School, Boston, Massachusetts*
[6]*Department of Biology, Loyola Marymount University, Los Angeles, California*
[7]*Department of Chemistry and Biochemistry, University of California at Los Angeles, Los Angeles, California*
[8]*Department of Cell and Molecular Biology, University of Texas at San Antonio, San Antonio, Texas*
[9]*Center for Computational and Integrative Biology, Massachusetts General Hospital and Harvard Medical School, Boston, Massachusetts*

ABSTRACT

Meiosis1 arresting protein (*M1ap*) is a novel vertebrate gene expressed exclusively in germ cells of the embryonic ovary and the adult testis. In male mice, *M1ap* expression, which is present from spermatogonia to secondary spermatocytes, is evolutionarily conserved and has a specific spatial and temporal pattern suggestive of a role during germ cell development. To test its function, mice deficient in *M1ap* were created. Whereas females had histologically normal ovaries, males exhibited reduced testicular size and a myriad of tubular defects, which led to severe oligozoospermia and infertility. Although some germ cells arrested at the zygotene/pachytene stages, most cells advanced to metaphase I before arresting and entering apoptosis. Cells that reached metaphase I were unable to properly align their chromosomes at the metaphase plate due to abnormal chromosome synapses and failure to form crossover foci. Depending on the state of tubular degeneration, all germ cells, with the exemption of spermatogonia, disappeared; with further deterioration, tubules displaying only Sertoli cells reminiscent of Sertoli cell-only syndrome in humans were observed. Our results uncovered an essential role for *M1ap* as a novel germ cell gene not previously implicated in male germ cell development and suggest that mutations in *M1AP* could account for some cases of nonobstructive oligozoospermia in men.

infertility, meiosis, meiotic arrest, oligozoospermia, spermatogenesis, testis, vertebrates

INTRODUCTION

Approximately 10% of couples seek medical advice because of infertility, a frequency similar to conditions related to lifestyle-related diseases such as diabetes or hypertension [1]. The pathoetiology of infertility, which is divided equally between testis, ovary, and tubal defects, is estimated to affect 1 in 20 men; 30% of cases appear to have a genetic basis, often due to abnormalities affecting meiosis [2]. In fact, meiotic defects are thought to account for approximately 48% of nonobstructive azoospermia and severe oligozoospermia in men [3].

Male germ cells are among the most self-renewing cells in an animal and proliferate in an orderly fashion from the basal to the adluminal compartments within the germinal epithelium of the seminiferous tubules [4]. The basal and adluminal compartments are separated by the formation of tight junctions between Sertoli cells, which creates the blood-testis barrier [5, 6]. Spermatogonia and preleptotene cells are found within the basal compartment, whereas meiotic cells are localized in the adluminal section. Primary spermatocytes (meiosis I) differentiate sequentially during prophase I in four morphologically defined stages: leptotene, zygotene, pachytene, and diplotene. Diplotene cells then undergo the G_2/M transition, aligning their chromosomes at the metaphase I plate in anticipation of cell division and formation of secondary spermatocytes (meiosis II), which then divide once more in the absence of replication of DNA to form round spermatids that then differentiate first into elongating spermatids and then into spermatozoa.

These multiple mitotic and meiotic divisions not only lead to an excess in germ cells but also to germ cells acquiring chromosomal abnormalities. Depending on the nature of these mutations, cells could become developmentally arrested and eventually be removed mainly through apoptosis [7–9]. Abnormal germ cells can arrest at any time in their development, with the pachytene and metaphase I (spindle) checkpoints being the two common stages [10–12]. Proteins can influence meiosis directly, by localizing to the nucleus, where they can bind to chromosomes, or indirectly, without entering the nucleus [13–16]. Although mutations in meiosis genes lead to germ cell arrest and death, their molecular pathways are not always clear, and in many cases, the suspected interacting proteins have not yet been discovered. Identifying new genes encoding either for interacting proteins or for proteins that are part of novel pathways, as well as

[1]This work was supported in part by the SURDNA/GAR Fellowship Fund from the Department of Surgery, Massachusetts General Hospital, and NIH National Cancer Institute, supplement grant PA-05-015 to N.A.A. and research grant CA17393 to P.K.D.
[2]Correspondence and current address: Nelson A. Arango, Department of Dermatology, Boston University, 607 Albany St., Room 409, Boston, MA 02118. E-mail: aarango@bu.edu
[3]These authors contributed equally to this work.

Received: 28 December 2011.
First decision: 31 January 2012.
Accepted: 17 December 2012.

eISSN: 1529-7268 http://www.biolreprod.org
ISSN: 0006-3363

determining their role in human infertility, is critical for the prevention and treatment of this common affliction.

This paper describes meiosis 1 arresting protein (*M1ap*) as a novel germ cell gene required for meiosis I progression in males. *M1ap* was originally described by Jang et al. [17] while exploring for genes present within the nonrecombinant region of mnd2 on mouse chromosome 6, a region that has been linked to progressive neuromuscular degeneration. Based on a retroviral insertion mutagenesis study, *M1ap* was also found to synergize with Cbfb (core binding factor)-MYH11 (myosin, heavy chain 11) translocation during the onset of acute myeloid leukemia [18]. Despite these observations, a function for *M1ap* in either neuromuscular disorders or acute myeloid leukemia could not be deciphered, because expression could not be detected in any of the adult tissues affected by the disease. Although originally named *D6Mm5e* (DNA segment, Chr. 6, Miriam Meisler 5, expressed), we have renamed this gene *M1ap* based on our previous findings [19] and those reported herein. Although *M1ap* is expressed in both the male and female germline, we found it to be critical for the development of germ cells in males, because the majority of *M1ap*-deficient spermatocytes are eliminated via apoptosis either at the pachytene checkpoint or later at the spindle checkpoint during metaphase I.

MATERIALS AND METHODS

RNA Extraction and Semiquantitative and Quantitative RT-PCR

Total RNA from postnatal mouse testes was isolated by homogenization with TRIzol (Invitrogen) and quantitated by absorbance at 260 nm. Semiquantitative RT–PCR was performed using *M1ap* primers to exon 7 (5′-CTGCCTGCAGCTTCTATGTG-3′) and 3′ untranslated region (5′-CAGCGT CAGAAGAGGAAGAG-3′). *Gapdh* primers (5′-TCCACCACCCTGTTGCTG TA-3′) and (5′-ACCACAGTCCATGCCATCAC-3′) were used as an internal control. Reverse transcription was performed at 42°C for 90 min using Reverse iT 1st Strand Synthesis Kit (Abgene). PCR conditions were as follows: 94°C initial denaturation for 1 min, followed by 30 cycles (*M1ap*) or 25 cycles (glyceraldehyde 3-phosphate dehydrogenase [*Gapdh*]) of PCR at 94°C for 30 sec, 60°C for 30 sec, and 72°C for 1 min. The PCR products were then electrophoresed in 1% agarose gel and stained with ethidium bromide.

Highly enriched populations of specific spermatogenic cell types were recovered using the StaPut gradient technique as previously described [20, 21]. Briefly, testes were dissected from male mice at different ages, decapsulated, and then enzymatically dissociated using collagenase and trypsin. Cells were loaded onto a 2%–4% continuous gradient of bovine serum albumin (BSA) and allowed to settle for approximate 4 h. The gradient was fractionated, and those fractions containing each desired cell type were pooled. Primitive type A spermatogonia and Sertoli cells were isolated from testes of mice at Postnatal Day (P) 6. Separate populations of type A and type B spermatogonia were recovered from P8 testes. Preleptotene spermatocytes, a combined population of leptotene plus zygotene spermatocytes, and a population of early pachytene spermatocytes were recovered from juvenile males at P18, and a population of adult pachytene spermatocytes, round spermatids, and elongating spermatids plus residual bodies were recovered from males after P60. Populations of spermatogonia and juvenile spermatocytes were enriched to a purity of 85% or greater, whereas adult spermatocytes and spermatids were enriched to a purity of 95% or greater, all as judged by cellular morphological characteristics under phase optics. Total RNA was then prepared from each enriched population using TRIzol reagent following the manufacturer's instructions. Purity and quality of the resulting RNA were determined on the basis of a continuous scan of ultraviolet absorption patterns at 220–320 nm as well as by visualization of intact RNA (including intact bands of ribosomal RNAs) following electrophoresis through 1% denaturing agarose. RNA was reverse transcribed as described above.

Quantitative RT-PCR was performed using the CFX96 Real-Time PCR System (Bio-Rad) with SYBR Green PCR Mastermix (Applied Biosystems). Final data were presented as the average number from triplicates. *Gapdh* was used as reference gene for the comparative CT or standard curve method for relative quantitation of gene expression with forward 5′-TGCGACTTCAA CAGCAACTC-3′ and reverse 5′-GGACACTGAGCAAGAGAGGC-3′ primers. *M1ap* was amplified using forward 5′-GCCTTACTACCCCTGGCAAT-3′ and reverse 5′-TGTCAGAAGACTGCAGGTGG-3′ primers.

Western Blot Analysis

Samples were homogenized in RIPA buffer (50 mM Tris-HCl [PH 8.0], 150 mM NaCl, 1% NP-40, 0.5% sodium deoxycholate, 0.1% SDS, and one Mini Protease Inhibitor Cocktail Tablet [Roche Diagnostics]). Lysate samples were cleared by centrifugation at 14 000 RPM for 15 min, and the supernatants were used for Western blot analysis. Protein concentration was determined using the Coomassie Plus (Bradford) Assay (Thermo Scientific Co.). The supernatants (10–20 mg) were reduced with 2.5% β-mercaptoethanol (0.325 M) in 1× Laemmli buffer (0.0625 mM Tris [pH 6.8], 2% [w/v] SDS stock, 10% [v/v] glycerol, and 0.002% [w/v] bromophenol blue) and heat denatured on a thermoblock at 70°C for 10 min. Lysate samples were run on a NuPAGE Novex 4%–12% Tris-Bis Midi-Gel (Invitrogen) at 130 V with 1× MES Running Buffer (Invitrogen).

For Western blot analysis, gels were transferred onto polyvinylidene fluoride membranes (Millipore) previously equilibrated in 1× NuPAGE Transfer Buffer (Invitrogen) containing 12% (v/v) methanol at 25 V for 45 min and at 35 V for another 45 min. Membranes were blocked with 1× PBS and 0.1% Tween-20 containing 5% nonfat dry milk for 30 min at room temperature and probed with the rabbit polyclonal anti-M1AP (1:1000 in blocking buffer overnight at 4°C) developed in our laboratory against a synthetic peptide. The antibody was affinity-purified using a SulfoLink matrix (Pierce). Blots were washed two times for 5 min each time at room temperature with 1× PBS and 0.1% Tween-20. Thereafter, the blots were incubated with horseradish peroxidase-conjugated secondary antibody (1:100 000 in 1× PBS and 0.1% Tween-20) for 45 min at room temperature. Blots were washed three times for 5 min each time at room temperature with 1× PBS and 0.1% Tween-20. Proteins were visualized with the ECL kit detection system (PerkinElmer) onto BioMax MR film (Kodak). The membranes were stripped and reprobed with a rabbit anti-β-actin (1:1000 in blocking buffer overnight at 4°C; Abcam).

Generation of Gene-Trapped Embryonic Stem Cell Clone and Germline Transmission

All animal protocols were approved by the Massachusetts General Hospital Institutional Animal Care and Use Committee. The trapped embryonic stem (ES) cell line (RR0290) was generated at Bay Genomics and the International Gene Trap Consortium (http://baygenomics.ucsf.edu), and the exact site of insertion of the gene-trap vector (β-geo) was determined by reverse PCR as previously described [22]. The trapped ES cell clone was injected into C57BL/6 (B6) blastocysts and transferred into the uteri of Swiss foster mothers at 2.5 days postcoitum. Male chimeras were bred to B6 females, and their agouti offspring were genotyped to confirm germline transmission of the trapped allele by PCR with primers for the wild-type *M1ap* allele, M1apF (5′-ATCTGGCGTGTGGTTTACAC-3′) and M1apR (5′-CTGACTCCTG TAAGTTGTCC-3′), and trapped *M1ap* allele, M1apInvF (5′-TCGTGCACC CAACTGATCTTC-3′) and M1apR (5′-CTGACTCCTGTAAGTTGTCC-3′). PCR conditions were as follows: 94°C initial denaturation for 1 min, followed by 30 cycles of PCR at 94°C for 30 sec, 60°C for 30 sec, and 72°C for 1 min. The PCR products were then electrophoresed in 2% agarose gel and stained with ethidium bromide.

β-Galactosidase Staining

Embryos were dissected at Embryonic Day (E) 14.5, their upper trunks removed, and their abdomens opened for better reagent penetration before placing them in 4% paraformaldehyde at 4°C for 30–45 min. Adult testes were dissected before fixation either intact or after the tunica albuginea was removed, and the seminiferous tubules were extruded from the testes. Isolated seminiferous tubules were enzymatically dissociated using collagenase and trypsin. The embryos, testes, and isolated seminiferous tubules were processed for X-gal staining overnight at room temperature as previously described [23]. X-gal-stained tissues were postfixed overnight in 4% paraformaldehyde at 4°C. For histology, tissues were dehydrated in alcohol, cleared with xylene, and embedded in paraffin. Sections (section thickness, 7 μm) were cut and counterstained with eosin-Y.

Section In Situ Hybridization and Histology

For in situ hybridization (ISH), adult testes were harvested and then fixed overnight at 4°C in 4% paraformaldehyde. The tissues were dehydrated and embedded in paraffin, and serial sections (section thickness, 7 μm) were

generated. Tissue sections were rehydrated in graded alcohol, washed in PBT (PBS plus 0.1% Tween 20), and treated with 10 mg/ml of proteinase K for 10 min at room temperature. Slides were then refixed in 4% paraformaldehyde and treated with acetic anhydride in 0.1 M triethanolamine for 15 min. The sections were prehybridized for 1 h before hybridizing with either a 577-bp or full-length (1940-bp) sense or antisense *M1ap* digoxigenin-labeled riboprobes (1 ng/ml) overnight at 70°C. After hybridization, samples were blocked in 10% sheep serum for 1.5 h at room temperature and then incubated with anti-digoxigenin-alkaline phosphatase (AP) antibody (1:1000) overnight at 4°C. The resultant hybrids were detected with AP-coupled anti-digoxigenin antibodies and BM Purple colorimetric solution (Roche Pharmaceuticals).

For histological analyses, the testes were fixed for 4–6 h in Bouin solution, then embedded in paraffin, sectioned (section thickness, 7 μm), and stained with hematoxylin and eosin-Y using standard histological techniques.

Chromosome Spreads and Immunofluorescence

Surface-spread spermatocytes were obtained from P21 and P28 mice as previously described [24]. In brief, testes were dissected, and the tunica albuginea was removed to release the seminiferous tubules. The tubules were then minced with forceps in cold PBS. The preparation was left untouched for 1 min to allow large tissue pieces to sediment. The supernatant was transferred to an Eppendorf tube and centrifuged for 1 min at 14 000 RPM. The pelleted cells were resuspended and incubated for 30 min in a hypotonic solution. Cells were again pelleted and resuspended in 100 μM sucrose (pH 8.2). Twenty-milliliter drops were placed and spread on a slides pretreated with 2% paraformaldehyde and 0.15% Triton X-100 in PBS (pH 9.2). Slides were placed for 2 h in a humid chamber at room temperature, followed by three washes for 1 min each time in 0.4% PhotoFlo (Kodak). Slides were stored at −80°C until further use.

For immunofluorescence (IF) of chromosome spreads, slides were brought to room temperature before being rinsed in PBT and then blocked in 10% goat serum for 1 h. Slides were incubated with rabbit anti-SYCP3 (1:200; Abcam) for 2–3 h at room temperature, then washed three times in PBT 5 min each before incubation overnight at 4°C with either mouse anti-γH2AX (1:200; Abcam), mouse anti-SYCP1 (1:50; a kind gift from Dr. Howard Cooke), or mouse anti-MLH1 (1:200; Abcam). Slides were incubated with secondary antibodies, goat anti-rabbit (1:200) and goat anti-mouse (1:200; both from Jackson ImmunoResearch) for 1 h.

For IF of paraffin-embedded tissues, the testes were fixed for 4–6 h in Bouin solution, followed by a graded sucrose/PBS treatment (10%, 20%, 25%, and 30%). Tissues were embedded in paraffin and sectioned (section thickness, 7 μm). Sections were blocked in 10% goat serum in PBS for 1 h and then incubated at room temperature with rabbit anti-VASA antibody (Abcam) at a dilution of 1:200 for 2–3 h. Slides were washed in 3× PBS for 5 min each time before incubation overnight at 4°C with rat anti-germ cell nuclear antigen 1 (GCNA1) antibody (a kind gift from Dr. George Enders) at a dilution of 1:50. Slides were incubated with secondary goat anti-rabbit fluorescein isothiocyanate (1:200) and goat anti-rat Cy3 (1:200; both from Jackson ImmunoResearch) for 1 h.

Isolation of Mitochondria and Submitochondria Localization

HEK293 cells or F9 cells were cultured in Dulbecco modified Eagle medium supplemented with 10% fetal bovine serum (Gibco). Twenty-four hours after plating, HEK293 or F9 cells were either transfected with EGFPN1 or M1CP-EGFPN1 plasmid DNA using BioT transfection reagent (Bioland Scientific) and Lipofectamine (Invitrogen), respectively, or left untransfected. Twenty-four hours posttransfection, cells were scraped and pelleted at $800 \times g$ for 5 min in a benchtop centrifuge (Eppendorf 5810R). The pellet was washed once with PBS and resuspended in solution A supplemented with protease inhibitors (20 mM Hepes [pH 7.6], 220 mM mannitol, 70 mM sucrose, 1 mM ethylenediaminetetra-acetic acid, and 2 mg/ml of BSA). The suspension was dounced in a glass homogenizer using a tight-fitting, drill-fitted pestle (Wheaton). Following centrifugation at $800 \times g$ for 5 min, the pellet was discarded, and the supernatant containing mitochondria, microsomes, and cytosol was further centrifuged at $10\,000 \times g$ for 10 min in the cold. The supernatant (cytosol) and the pellet mitochondrial-enriched fraction (Mito) was resuspended in solution A (containing no BSA) and recentrifuged at $10\,000 \times g$ for 10 min. Concentration of mitochondrial fraction was estimated using the standard BCA assay (Pierce Chemical Co.).

Blots were probed with antibodies to green fluorescent protein (GFP; Abcam), Tubulin (Covance), Tom40, Tom20 (both from Santa Cruz Biotechnology, Inc.), and Mortalin (NeuroMab Antibodies, Inc.). Blots were developed with horseradish peroxidase secondary antibody and chemiluminescence (Thermo Scientific).

Microscopy

HEK293 or F9 cells transiently transfected with either EGFPN1 or M1CP-EGFPN1 were stained with MitoTracker Red CMXRos (Invitrogen) 24 h posttransfection. Fluorescence microscopy was performed with a microscope (Axiovert 200M; Carl Zeiss, Inc.) using a Plan-NeoFluar 63× NA oil objective. Images were acquired at room temperature (24°C) with a charge-coupled device camera (ORCA ER; Hamamatsu Photonics) controlled by Axiovision software (Carl Zeiss, Inc.). Image files were processed with PhotoShop software (Adobe). Scale bar represents 40 μm in Supplemental Figure S1.

RESULTS

M1ap *Expression in Postnatal Testis*

We have previously reported that in the embryo, *M1ap* expression is restricted to the germ cells of the XX gonad between E13.5 and E16.5, where it is seen as an anterior-to-posterior wave typical of meiotic genes [19]. Postnatally, expression becomes restricted to the testes, further demonstrating that *M1ap* is a meiotic gene [19]. To characterize further the expression of *M1ap* during male germ cell development, we conducted PCR assays on RNA isolated from whole testes at different postnatal time points (Fig. 1A) and on RNA from enriched populations of specific spermatogenic cell types (Fig. 1B). RT-PCR analyses of RNA extracted from whole testes revealed the onset of *M1ap* expression by P7 (Fig. 1A). In the absence of an antibody that works in tissue sections, we conducted quantitative RT-PCR on RNA isolated from enriched populations of specific spermatogenic cell types to determine the cell specificity of *M1ap* expression (Fig. 1B). As expected, *M1ap* transcripts were absent from Sertoli cells. Transcription of *M1ap* first appeared in type A spermatogonia, peaked in type B spermatogonia, then decreased to lower, yet still significant, levels in primary spermatocytes. *M1ap* expression was once again upregulated in spermatids, where levels reached about half those seen in type B spermatogonia.

M1AP Is a Cytosolic Protein

A highly conserved protein, M1AP has 42% identity between fish and human and 70% identity between mouse and human. Despite this, no protein signature domains, other than a mitochondria signal at its N-terminus, can be discerned. Although the mitochondria signal is well conserved across species, transfection with a *M1ap*-GFP into HELA (not shown) and HEK293 cells showed a diffuse cytoplasmic signal (Supplemental Fig. S1A; all supplemental data are available online at www.biolreprod.org). This was further corroborated by fractionation of transfected cells to isolate the mitochondria from the cytosol. Western blot analysis with an antibody against GFP only detects a signal in the cytoplasmic fraction (Supplemental Fig. S1B). Because M1AP expression is specific to germ cells, its subcellular localization could be different in these cells. For example, *Spo11*, a germ cell-specific gene that introduces double strand break (DSB) in DNA, is seen diffusely throughout the cytosol when overexpressed in HEK293 cells [25]. However, transfection with a *M1ap*-GFP plasmid into the germ cell line F9, in conjunction with fractionation of these transfected cells, showed only cytoplasmic expression (Supplemental Fig. S1) [26]. Thus, we conclude that although well conserved, the mitochondria signal is not functional in germ cells. Nonetheless, the spatial and temporal expression of *M1ap* as well as its high level of evolutionary conservation [19] suggested a role for *M1ap* during male germ cell development. To test its function, a mouse deficient in *M1ap* was created.

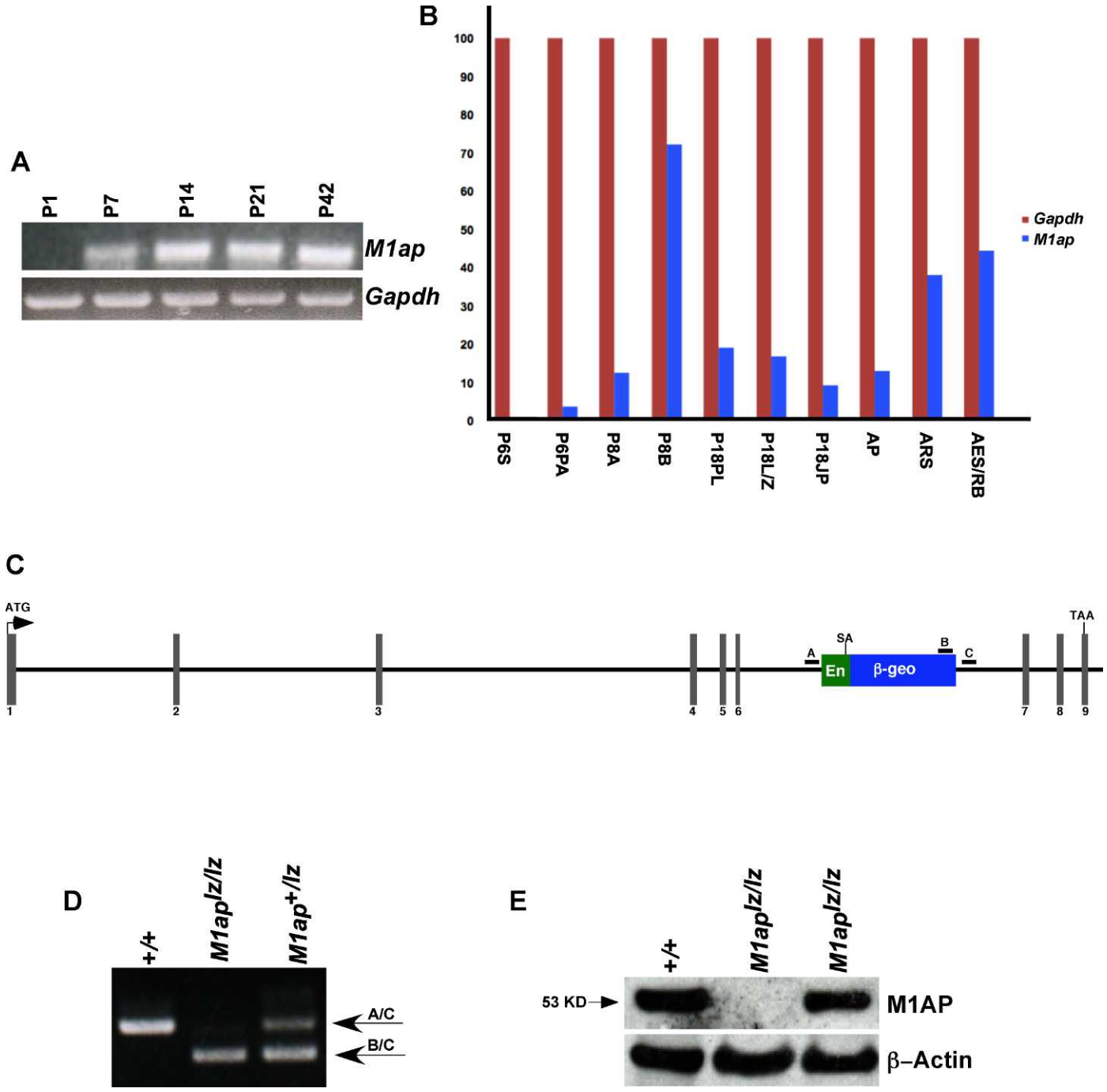

FIG. 1. *M1ap* expression and gene disruption strategy. **A**) RT-PCR analyses of postnatal testes showing the onset of *M1ap* expression by P7. *Gapdh* was used as loading control. **B**) Quantitative RT-PCR analyses of *M1ap* expression in specific spermatogenic cell types. The highest expression of *M1ap* is seen in P8 type B spermatogonia and spermatids of adult mice. A, type A spermatogonia; AES/RB, adult elongated spermatids/residual bodies; AP, adult pachytene; ARS, adult round spermatids; B, type B spermatogonia; JP, juvenile pachytene; L/Z, leptotene/zygotene; PA, primitive type A spermatogonia; PL, preleptotene; S, Sertoli cells. **C**) Gene disruption by gene-trapping methods. The mutant allele ($M1ap^{lz}$) was produced by inserting a β-geo cassette into intron 6. The β-geo cassette contains a splice acceptor (SA) capable of fusing to the splice donor of the preceding exon. A, B, and C represent the position within the genome of the primers used for mouse genotyping. ATG, start codon; TAA, stop codon. **D**) Genotyping strategy. Primers A, B, and C were used in a single PCR reaction. Wild-type allele = 358 bp; mutant allele = 296 bp. **E**) Western blot showing different levels of M1AP protein expression (~53 kDa) in wild-type (+/+) and $M1ap^{lz/lz}$ testes. β-Actin was used as loading control.

Generation and Characterization of the M1ap *Mutant Allele*

The creation of a mouse line deficient in *M1ap* was facilitated by the availability of a targeted ES cell line generated by gene-trapping methods at Bay Genomics and the International Gene Trap Consortium (http://baygenomics.ucsf.edu). Mouse *M1ap* is composed of nine exons spanning approximately 73 kb of genomic sequence. Because *M1ap* was disrupted by the introduction of a *lacZ*-neomycin (β-geo) cassette into intron 6, we herein refer to this allele as $M1ap^{lz}$ (Fig. 1C). To determine the exact integration site of the β-geo

cassette within exon 6, we performed inverse PCR (data not shown). This technique allows the amplification of DNA fragments that lie outside of known β-geo cassette sequences [22]. This in turn permitted us to develop a reliable PCR-based screen for the genotyping of $M1ap^{lz}$ mice (Fig. 1D). The β-geo cassette contains a splice acceptor sequence that allows fusion of the first six exons of *M1ap* with the β-geo cassette, thus producing a trapped allele (Fig. 1C). Whereas this fusion can happen with near 100% efficiency in some trapped genes, in the case of the $M1ap^{lz}$ allele we obtained mice exhibiting variable efficiency of the β-geo splice event, therefore giving rise to some mice with no apparent wild-type protein and others that still produced reduced levels of the protein (Fig. 1E). This allele is therefore a hypomorphic allele with variable expression, which proved to be very useful in subsequent phenotypic analyses.

We then tested whether the $M1ap^{lz}$ allele recapitulated the known endogenous expression of *M1ap* by following the expression of M1AP protein-based β-galactosidase (β-gal) activity. In mice, spermatogenesis commences at approximately P3, as gonocytes migrate from the center of the seminiferous tubules to the periphery and differentiate into type A spermatogonia [27]. This is succeeded by the formation of type B spermatogonia by P8. The first meiotic cells (leptotene) are first observed by P10, followed by zygotene, pachytene, and secondary spermatocytes by P12, P14, and P18, respectively [20]. In accord with our previously published ISH data, embryonic ovaries (Supplemental Fig. S2A) and adult testes (Supplemental Fig. S2, B–D) were positive for β-gal [19]. Interestingly, in adult testes, $M1ap^{lz}$ showed a cyclical pattern of β-gal activity in the seminiferous tubules indicative of a tight regulation of expression in a narrow subset of germ cells (Supplemental Fig. S2, B–D). Furthermore, β-gal expression was restricted to cells localized within the first couple of layers from the basement membrane (Supplemental Fig. S2D). This was contradictory to our previously published ISH data, in which transcripts were only detected in round and elongated spermatids [19]. To clarify this, we compared the endogenous expression of the *M1ap* RNA to that of the M1AP-β-gal fusion protein from the $M1ap^{lz}$ allele during prepubertal time points as well as before (P14) and just at the time that spermatids begin to appear (P21) (Supplemental Fig. S3). At P14, both *M1ap* RNA and M1AP-β-gal fusion protein localized to the basal and adluminal compartments of the seminiferous tubules. However, by P21, expression was only found at the periphery of the tubules. In addition, not all tubules were positive for either RNA or β-gal at both developmental stages.

Deficiency in M1ap *Results in a Wide Range of Tubular Defects as Early as P14*

Despite *M1ap* being expressed in germ cells of both sexes, $M1ap^{lz/lz}$ ovaries appeared normal, whereas $M1ap^{lz/lz}$ testes were riddled with tubular defects, which led to severe oligozoospermia and infertility. $M1ap^{lz/lz}$ males showed normal copulatory behavior, and their internal reproductive organs, as well as their ability to plug, was similar to controls, indicating that the hypothalamus-pituitary-gonadal axis was not disrupted and that the defects were intrinsic to the testes (data not shown). Because of the hypomorphic nature of the allele, $M1ap^{lz/lz}$ testes varied in size and weight. Adult testes from the most affected $M1ap^{lz/lz}$ animals weighed approximately 50% less than controls (Fig. 2A). As expected, histological sections of $M1ap^{lz/lz}$ testes also showed a variation in the percentage of affected tubules and the degree of tubular degeneration (Fig. 2 and Supplemental Fig. S4). Specifically, we observed vacuolization, tubules with no germ cells beyond the zygotene/pachytene stages, tubules populated by abnormal metaphase I cells with misaligned chromosomes at the metaphase plate, and decreased tubular diameter (Fig. 2, D, E, G, and H, and Supplemental Fig. S3, C–F). In tubules with a higher degree of degeneration, all cells, with the exception of spermatogonia and Sertoli cells, disappeared (Supplemental Fig. S4F). As the tubules deteriorated further, Sertoli cell-only (SCO) tubules were observed, and in some instances, Sertoli cell nuclei were found toward the lumen (Fig. 2H). In some tubules, spermatogonia were seen in the adluminal compartment (Supplemental Fig. S4F). Interestingly, even in the most affected mice, a few spermatids were detected (Supplemental Fig. S4E). A few elongated spermatids were also found in the epididymides of some of these mice, where they were accompanied by desquamated round germ cells, some of which had a pyknotic nuclei appearance suggestive of apoptosis (Fig. 2F).

To characterize the onset of the germ cell defect, we analyzed testes chronologically at different stages of postnatal development (Fig. 3). Consistent with the observation that the highest expression of *M1ap* is first observed in P8 type B spermatogonia, no differences were observed in sections of P7 $M1ap^{lz/lz}$ testes when compared to controls (data not shown). The first anomalies in germ cell development were seen by P14, when some tubules appeared to be devoid of meiotic germ cells (Fig. 3A). This was confirmed by IF with antibodies against mouse vasa homologue (MVH), which is expressed in spermatogonia and primary and secondary spermatocytes [28], and GCNA1, which is expressed strongly in spermatogonia and early spermatocytes and more weakly in late spermatocytes [29] (Fig. 3A). A more dramatic alteration in spermatogenesis was observed by P21 (Fig. 3B and Supplemental Fig. S5). At this age, testes from $M1ap^{lz/lz}$ mice contained germ cells with highly condensed chromatin (leptotene/zygotene), which are normally present within a couple of layers from the basement membrane, farther inside the adluminal compartment (Figs. 3B and Supplemental Fig. S5B). Tubules with accumulating metaphase I cells were observed as well (Fig. 3B), as was a reduction in late primary spermatocytes (pachytene/diplotene) as determined by a marked decreased in MVH-positive germ cells and an increase in the amount of germ cells staining strongly for GCNA1 (Fig. 3B). In addition, the localization of the GCNA1-positive germ cells within the germinal epithelium was abnormal, indicating a continual buildup of meiosis I germ cells that were unable to maintain their differentiation abilities. In tubules with a more advanced state of degeneration, spermatogonia cells, which are normally present in the basal compartment, were seen away from the basement membrane (Supplemental Fig. S5C). Although few round spermatids were observed in these mice, the overall secondary spermatocyte population was heavily compromised. By P28, $M1ap^{lz/lz}$ testes exhibited a severe absence of secondary spermatocytes and a significant reduction in tubular diameter (Fig. 3C). In addition, tubules containing germ cells arrested at metaphase I were readily observed, as were tubules with germ cells arrested at the zygotene/pachytene stages. Depletion of MVH-positive cells and abnormal localization of GCNA1-expressing cells were detected in some tubules (Fig. 3C). By P56, $M1ap^{lz/lz}$ mice also exhibited depletion of secondary spermatocytes, an increase in zygotene/pachytene cells, abnormal metaphase I cells, a reduction in tubular diameter, and the presence of SCO tubules (Fig. 3D). Cells with strong GCNA1 signal, normally present near the periphery of the tubule, were seen a few layers inside the adluminal compartment (Fig. 3D). Furthermore, some tubules contained few MVH-positive cells, whereas others

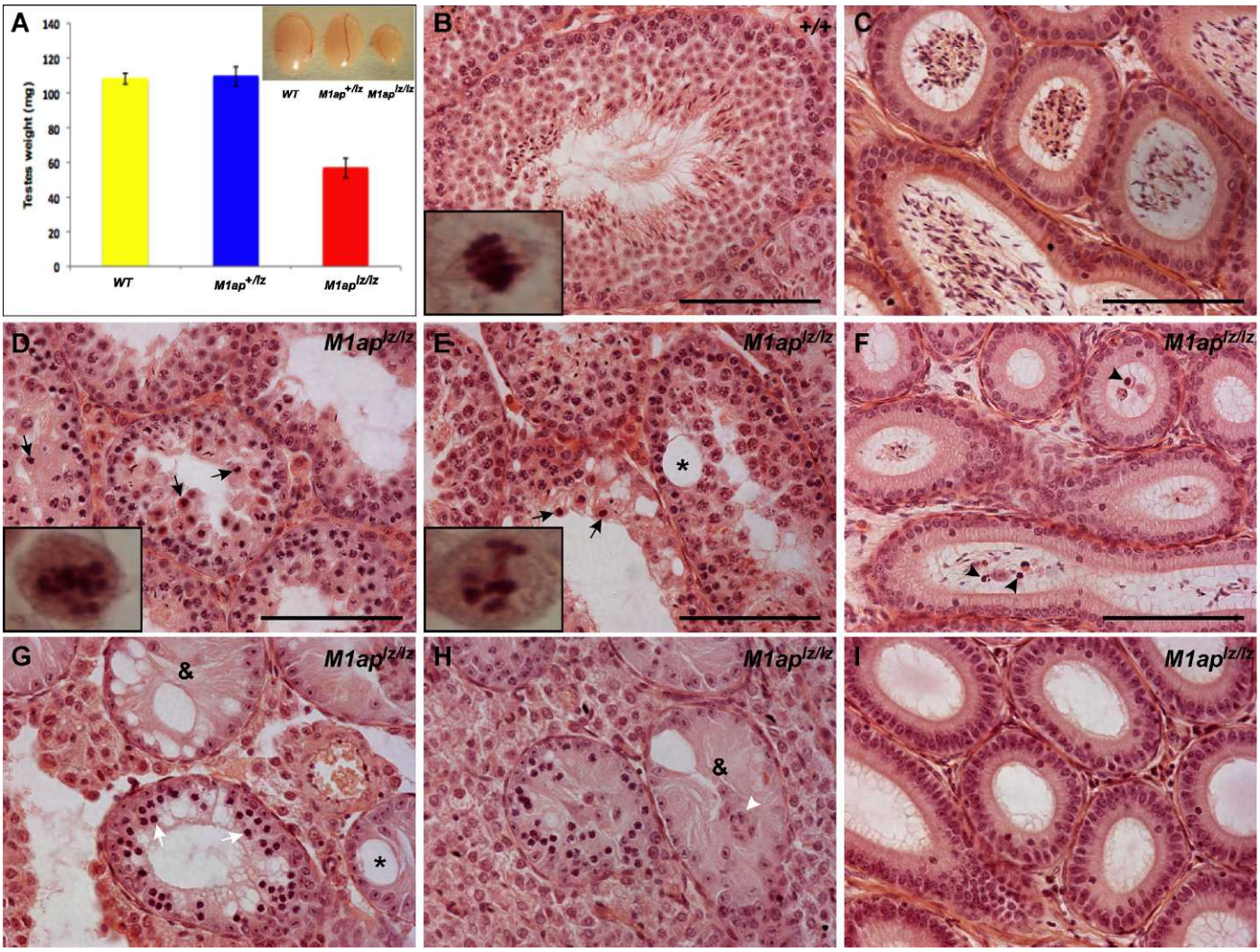

FIG. 2. Decreased testicular weight and multiple tubular defects in *M1ap*-deficient mice. **A**) Testes from $M1ap^{lz/lz}$ mice exhibit an approximately 50% reduction in weight compared to wild-type and heterozygous mice. **B–I**) Multiple histological abnormalities in adult $M1ap^{lz/lz}$ testes. **B** and **C**) Sections of wild-type (+/+) testis and corresponding epididymis showing normal spermatogenesis. Inset in **B** shows metaphase cell. **D–F**) $M1ap^{lz/lz}$ testis sections illustrating abnormal metaphase I cells (arrows), vacuolization (asterisk), and an overall reduction in secondary spermatocytes and tubular diameter. The drastic decrease in secondary spermatocytes is evident in the corresponding epididymis, where very few elongated spermatids are found. Round spermatocytes are also visible, some of which show characteristics of apoptosis (arrowheads in **F**). Insets in **D** and **E** show misaligned chromosomes at metaphase I plate. **G** and **H**) $M1ap^{lz/lz}$ testis sections detailing tubules containing no germ cells beyond zygotene stages (white arrows), vacuolization (asterisk), Sertoli cell clusters in the center of the tubule (white arrowhead), and SCO tubules (&). **I**) No spermatozoa are detected in the corresponding epididymis. Bar = 100 μm.

were negative for MVH and GCNA1, confirming the presence of SOC tubules. Overall, $M1ap^{lz/lz}$ mice expressing higher levels of wild-type *M1ap* (weak hypomorph) showed a more abundant presence of metaphase I arrest, whereas $M1ap^{lz/lz}$ mice expressing lower levels of wild-type *M1ap* (strong hypomorph) had fewer metaphase I cells and more developmentally immature germ cells represented by highly condensed chromatin (zygotene) as well as pachytene cells. In general, these mice contained a highly disorganized germinal epithelium.

Abnormal Chromosome Behavior Leads to Apoptosis in $M1ap^{lz/lz}$ *Mice*

Meiotic recombination is a highly complex process required for gamete formation. This encompasses a tight coordination of a myriad of proteins involved in DSB formation and repair, synapses, crossover, and segregation [12]. Thus, it is not surprising that mutations in genes regulating meiosis cause a wide spectrum of spermatogenic defects [30]. To investigate further the causes of the defect, we analyzed meiotic chromosome spreads of $M1ap^{lz/lz}$ mice by first using antibodies against the synaptonemal complex protein SYCP3, which paints the lateral/axial elements of synapsed and unsynapsed chromosomes, and histone variant γH2AX, which labels unrepaired DSBs and unsynapsed regions [31, 32]. SYCP3 binds to chromosomes at preleptotene and dissociates by anaphase I, whereas γH2AX appears during preleptotene, as DSBs are introduced, and disappears from autosomes by the late zygotene/pachytene stages, as chromosome synapses are completed and DSBs are repaired [32]. However, γH2AX remains attached to the partially synapsed X and Y chromosomes until the end of diplotene. In $M1ap^{lz/lz}$ testes, γH2AX signal was retained in the autosomes as late as diakinesis, indicating a failure to repair DSBs, properly synapse, and/or form crossovers (Fig. 4 and Supplemental

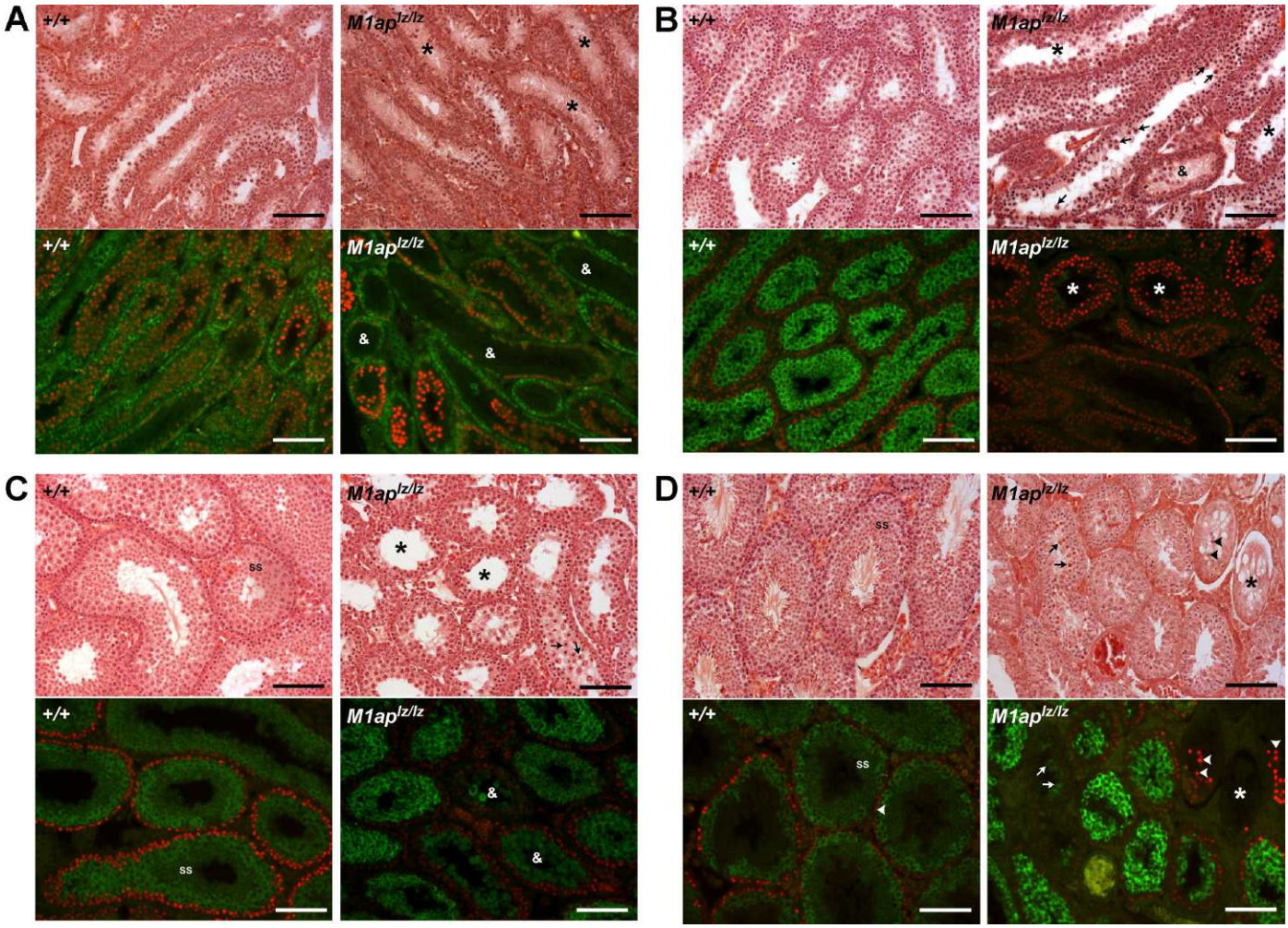

FIG. 3. Chronological analyses of *M1ap*$^{lz/lz}$ mice revealed testicular defects as early as P14. **A**) Hematoxylin and eosin-Y-stained sections of P14 *M1ap*$^{lz/lz}$ testes illustrating tubules devoid of meiotic germ cells (asterisks). IF showing a decrease of MVH-positive (green) and GCNA1-positive (red) cells (&). **B**) Sections of P21 *M1ap*$^{lz/lz}$ testes showing tubules with no meiotic germ cells beyond zygotene/pachytene stages (black asterisks), metaphase I arrested cells (arrows), and tubules containing only Sertoli cells and spermatogonia (&). A dramatic decrease is seen in cells expressing MVH, along with an abnormal distribution of GCNA1-positive cells (white asterisks). **C**) Sections of P28 *M1ap*$^{lz/lz}$ testes depicting multiple tubular defects. Some tubules are devoid of germ cells beyond the zygotene/pachytene stages (asterisk), whereas others have an abundance of abnormal metaphase I cells (arrows), all of which lead to a lack of secondary spermatocytes (SS). MVH and GCNA1 staining revealed a disorganized germinal epithelium containing degenerating tubules (&), reduced tubular diameter, and an absence of secondary spermatocytes (SS). **D**) Sections of P56 *M1ap*$^{lz/lz}$ testes showing a dramatic reduction in secondary spermatocytes (SS), abnormal metaphase I cells (arrows), SCO tubules (asterisks), and reduced tubular diameter. In addition, a decrease in germ cells expressing MVH and abnormal localization of GCNA1-positive germ cells (arrowheads) is seen. Bar = 100 μm.

Fig. S6). In addition, X-Y chromosome synapses were affected, and autosomes were involved in nonhomologous pairing (Fig. 4). Autosomal γH2AX signal has been shown to persist as late as diplonema in *Atm*$^{-/-}$; *Spo11*$^{+/-}$ spermatocytes but has not been reported at diakinesis [24]. Because prolonged retention of γH2AX has been linked to abnormal chromosome synapses and failed crossover foci formation, we investigated whether these two events were occurring normally in *M1ap*$^{lz/lz}$ spermatocytes. IF of *M1ap*$^{lz/lz}$ pachytene cells with antibodies against SYCP3 and SYCP1, which only labels paired chromosomes [33], confirmed the synapse defect (Fig. 5). SYCP3- and SYCP1-stained *M1ap*$^{lz/lz}$ spermatocytes showed abatement in homologous chromosome synapses; this loss of synaptonemal complex led to nonhomologous pairing and unsynapsed X-Y chromosomes (Fig. 4). We then looked at the ability of the *M1ap*$^{lz/lz}$ spermatocytes to form crossover foci, a required event for meiosis progression [33, 34]. IF with antibodies against SYCP3 and the mismatch repair protein MLH1, a marker of crossover foci, demonstrated that *M1ap*$^{lz/lz}$ germ cells were deficient in crossover foci formation (Fig. 6A). A range of approximately 40% (weak hypomorph) to 90% (strong hypomorph) of cells carried at least one chromosome without crossover foci. Furthermore, *M1ap*$^{lz/lz}$ cells expressing lower levels of wild-type M1AP (strong hypomorph) had an increase in chromosomes without crossover foci. To address whether the observed meiotic defects led to germ cell apoptosis, we conducted TUNEL analyses of testes sections. *M1ap*$^{lz/lz}$ testes showed a dramatic increase in apoptosis when compared to controls (Fig. 6B). Taken together, our data suggests that the spermatogenic arrest and subsequent apoptosis in *M1ap*$^{lz/lz}$ mice correlates with abnormal chromosome pairing and a failure to form crossover foci.

DISCUSSION

Expression of the M1ap^{lz} *Allele*

Our results showed that *M1ap* has a very dynamic and unique expression pattern during spermatogenesis. First, as

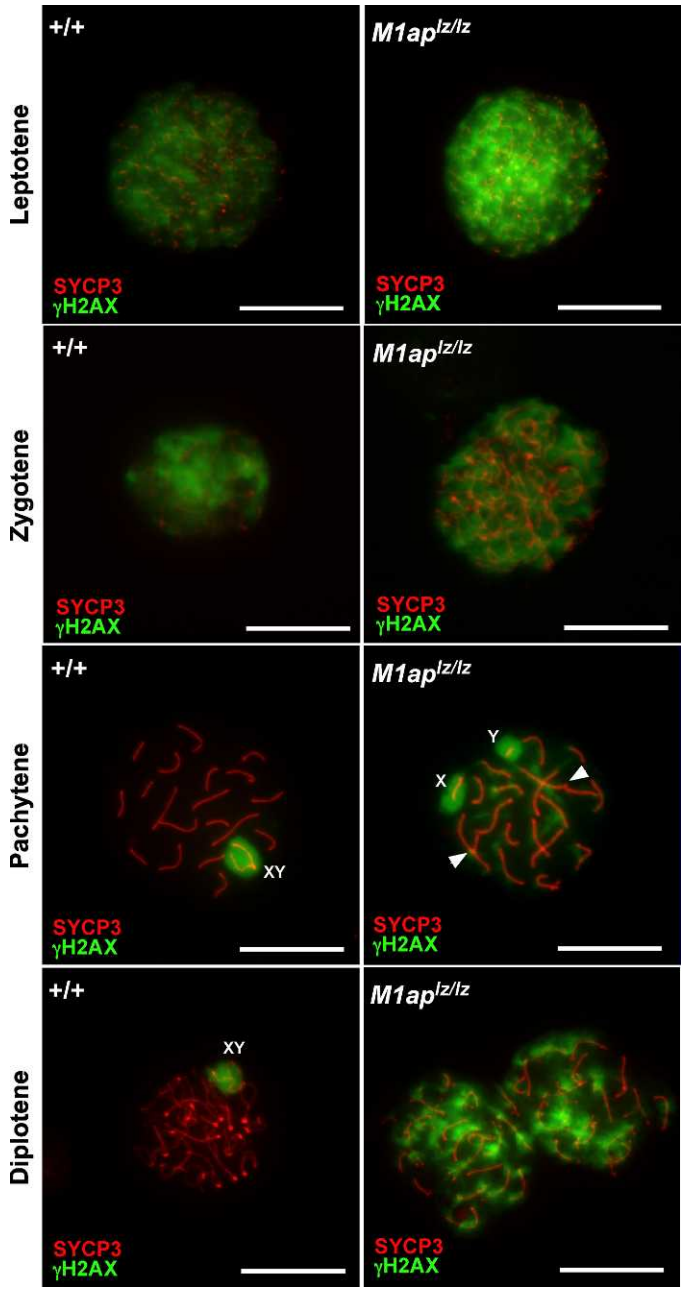

FIG. 4. Localization of γH2AX and SYCP3 protein in wild-type (+/+) and *M1ap*$^{lz/lz}$ spermatocytes. In wild-type spermatocytes, γH2AX disappears from autosomes by pachynema, whereas it remains in association with the XY body until the end of diplonema. In *M1ap*$^{lz/lz}$ spermatocytes, γH2AX signal is retained in the autosomes as late as diplonema. Nonhomologous pairing (arrowhead) and separate X-Y chromosomes are also commonly observed. Bar = 100 μm.

testes progress in postnatal development, RNA and protein expression in cells at the adluminal compartment ceases, whereas it remains at the periphery of the tubules. Second, a cyclical pattern of expression is present along the length of the tubules. This cyclical pattern of β-gal activity is not seen when the β-geo cassette is driven by genes highly expressed in round and elongating spermatids, as observed in mice carrying a β-geo-trapped *Jhdm2a* histone demethylase allele. In these mice, β-gal activity is detected throughout the entire length of the seminiferous tubules [35]. Thus, our data strongly suggest that the RNA expression pattern seen in the adults by ISH was the result of the RNA probes being sequestered by the numerous *M1ap*-expressing spermatids. In fact, in the adult testis, the majority of the cells found within the seminiferous tubules are spermatids. Translation of *M1ap* transcripts into protein appears not to take place in these cells. Alternatively, the presence of the β-geo cassette within M1AP alters the expression pattern of M1AP. We conclude that the *M1ap*^{lz} allele recapitulates the endogenous expression of *M1ap* in both males and females and can be used in cell mapping experiments.

Deficiency in M1ap *Results in a Wide Range of Tubular Defects as Early as P14*

The main cause of infertility in *M1ap*-deficient male mice is the inability of germ cells to progress passed meiosis I. However, even in the most affected *M1ap*$^{lz/lz}$ mice, some round and elongating spermatids were found within the tubules and, in some animals, also in the epididymides (Fig. 2, D–I). We conclude that *M1ap*$^{lz/lz}$ mice are severely oligozoospermic, but not azoospermic, as a result of the mode of action of *M1ap*. However, we cannot rule out that the observed oligozoospermia was instead due to the hypomorphic nature of the allele. Theoretically, the N-terminal portion of M1AP protein preceding the β-geo insertion should be expressed, translated, and recognized by the M1AP antibody. However, as shown in Figure 1E, the protein is not detected in mice carrying two copies of the trapped allele, which suggests the disappearance of either the RNA or the protein during its transcription or translation, respectively. As a result, we expect the mutant protein not to have any remaining function. Creation of a full knockout mouse by standard gene targeting methodologies can resolve these questions. Whereas numerous loss-of-function mutations in genes known to regulate meiosis in yeast and mammals result in full activation of the pachytene checkpoint, loss-of-function mutations in other meiosis genes lead to metaphase I arrest, primarily from an inability to properly align chromosomes at the metaphase plate [36, 37]. Both, topoisomerase II *Spo11* mutant mice and ataxia telangiectasia mutated (*Atm*) mice are infertile due to the inability of germ cells to progress beyond the pachytene stage [24, 38]. Interestingly, in *Atm*-null males carrying only one functional copy of *Spo11* (*Atm*$^{-/-}$; *Spo11*$^{+/-}$), prophase I is allowed to continue, and spermatocytes arrest instead at metaphase I [24]. Closer examination revealed a disorganized metaphase plate with few elongated spermatids. Mice deficient in E3 ubiquitin ligase (*Mei4* gene) also exhibit abnormal chromosome alignment at the metaphase I plate with subsequent activation of the spindle checkpoint at metaphase I [39]. Transgenic insertions have also yielded oligozoospermic infertile male mice displaying metaphase I arrest [40]. In addition, chromosomal abnormalities such as those seen in Robertsonian (Rb) translocations resulted in misaligned chromosomes at the metaphase I plate and subsequent activation of the spindle checkpoint [41]. Despite this arrest, few sperm, characterized by higher levels aneuploidism, were detected in Rb mice. In most respects, the observed phenotype in *M1ap*$^{lz/lz}$ mice is similar to those mentioned above. Although some *M1ap*$^{lz/lz}$ spermatocytes arrested at pachynema (Supplemental Fig. S4C), the majority were able to complete the G_2/M transition. However, they entered apoptosis at metaphase I due to abnormal chromosome alignment at the metaphase plate (Fig. 2, D and E, and Supplemental Fig. S4D). Because M1AP expression was localized to the cytoplasm without any detectable presence in

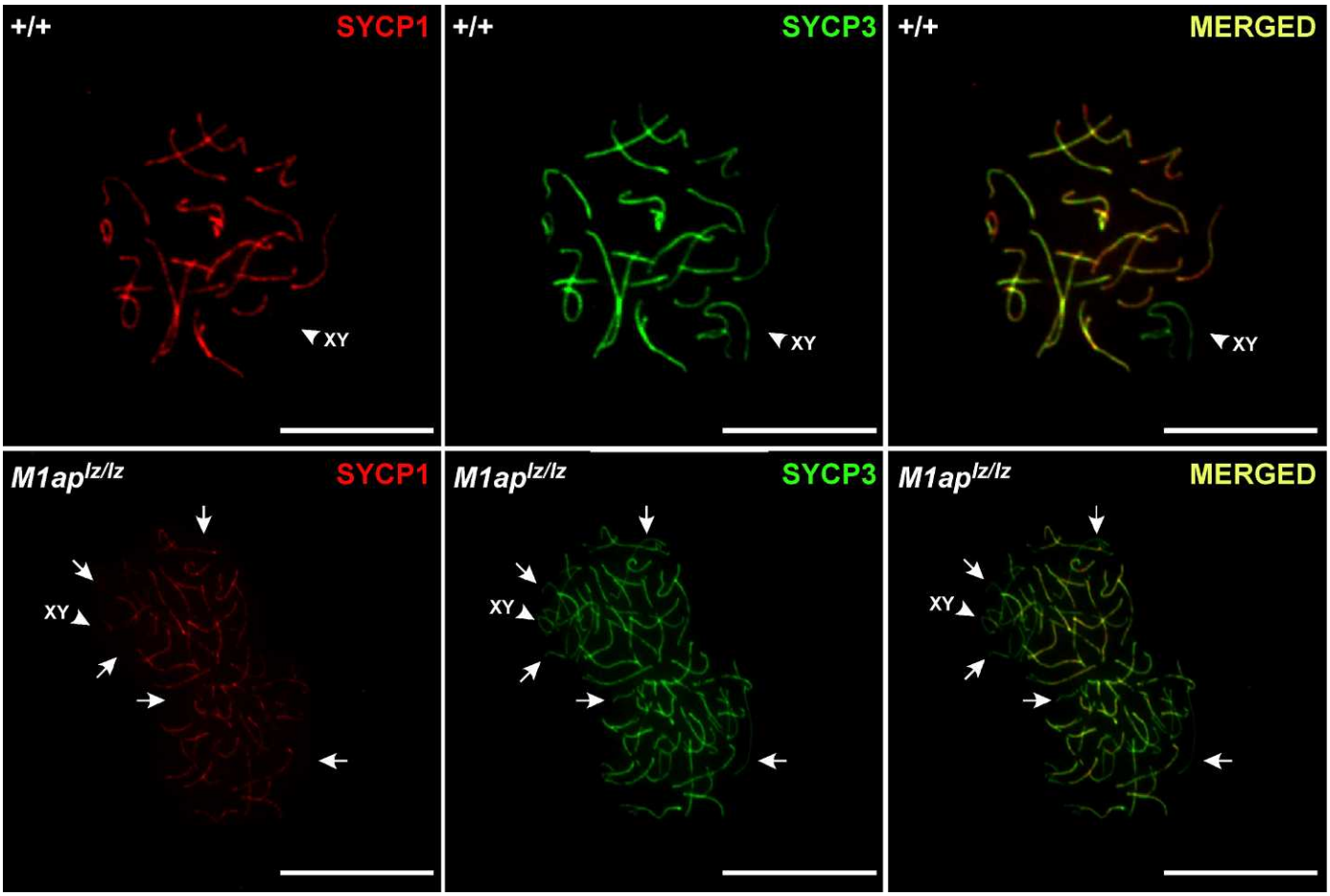

FIG. 5. Failed chromosome synapses in *M1ap*$^{lz/lz}$ spermatocytes. Whereas all chromosomes from wild-type (+/+) cells show SYCP1 signal (red) indicative of proper homologous pairing during pachynema, a proportion of chromosomes in *M1ap*$^{lz/lz}$ cells failed to synapse (arrows). Bar = 100 μm.

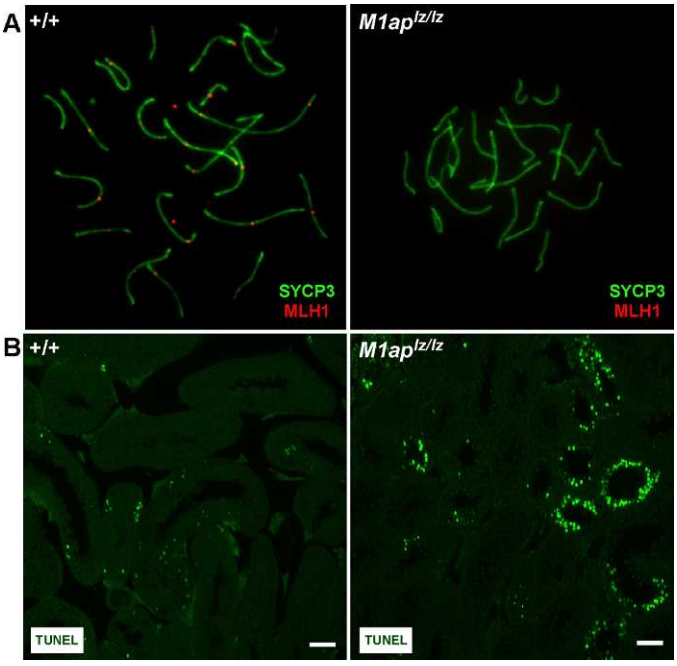

FIG. 6. Failed formation of crossover foci and increased apoptosis in *M1ap*$^{lz/lz}$ germ cells. **A**) *M1ap*$^{lz/lz}$ pachytene spermatocytes are deficient in MLH1 foci assembly (red). Original magnification ×1000. B) TUNEL assays revealed increased apoptosis in *M1ap*$^{lz/lz}$ testes. Bar = 100 μm.

the nucleus, we theorize that M1AP might be binding and activating a cytoplasmic protein that will then translocate into the nucleus to manage or repair DSBs. It will be important to study the exact mechanism by which *M1ap* regulates meiosis progression.

In summary, we have unequivocally shown that *M1ap* is essential for spermatogenesis, because disruption of *M1ap* function leads to multiple testicular abnormalities and severe oligozoospermia. Because animals as young as P21 show severe defects, we conclude that *M1ap* is necessary during the early stages of spermatogenesis.

Abnormal Chromosome Behavior Leads to Apoptosis in M1ap$^{lz/lz}$ *Mice*

A correlation has been suggested between the extent of synapses and crossover foci formation with the stages at which germ cells arrest and enter apoptosis [40, 42, 43]. Cells with extensive chromosome asynapses are normally destroyed at the pachytene checkpoint, whereas cells exhibiting milder asynapses but deficient in crossover foci formation can advance to metaphase I before arresting and entering apoptosis. Furthermore, the amount and location of crossover foci have been linked to random chromosome alignment at the metaphase I plate, leading to the activation of the spindle checkpoint [44, 45]. Mice deficient in crossover foci formation are either oligo- or azoospermic [24, 42]. Also, in mice deficient in meiotic chromosome pairing, germ cells are eliminated through

apoptosis at the pachytene and metaphase I checkpoints [46, 47]. Our results demonstrate that *M1ap*$^{lz/lz}$ spermatocytes containing unsynapsed chromosomes or reduced crossover foci are eliminated either at the pachytene checkpoint or at the spindle checkpoint of metaphase I.

The causes of male infertility are poorly understood. Approximately 400 mouse models leading to male infertility exist. Of those, more than 75 carry mutations in genes regulating germ cell development [30]. However, only a handful of these genes have been unequivocally implicated in infertility in men. Because the function of M1AP in mice is restricted to germ cells, and because M1AP is highly conserved across vertebrates, it will be important to screen for mutations in *M1AP* in infertile and subfertile men. In fact, severe oligozoospermia and azoospermia without any other developmental abnormalities is commonly observed in men. Equally important for potential translation to the clinic is the identification of M1AP-interacting proteins in mice and humans, because this may help us understand better the causes of the observed oligozoospermia in humans with clinical infertility. Further analysis of the function of *M1ap* will help to elucidate the process of male meiosis and causes of infertility in men.

ACKNOWLEDGMENT

We would like to thank David MacLaughlin and Kellee Siegfried for helpful discussion and critical review of the manuscript.

REFERENCES

1. de Kretser DM. Differences in the prevalence of cryptorchidism. Lancet 2004; 363:1250–1251.
2. McLachlan RI, Mallidis C, Ma K, Bhasin S, de Kretser DM. Genetic disorders and spermatogenesis. Reprod Fertil Dev 1998; 10:97–104.
3. Sun F, Turek P, Greene C, Ko E, Rademaker A, Martin RH. Abnormal progression through meiosis in men with nonobstructive azoospermia. Fertil Steril 2007; 87:565–571.
4. Setchell BP, Hertel T, Soder O. Postnatal testicular development, cellular organization and paracrine regulation. Endocr Dev 2003; 5:24–37.
5. Mruk DD, Cheng CY. Tight junctions in the testis: new perspectives. Philos Trans R Soc Lond B Biol Sci 2010; 365:1621–1635.
6. Setchell BP. Blood-testis barrier, junctional and transport proteins and spermatogenesis. Adv Exp Med Biol 2008; 636:212–233.
7. Baum JS, St George JP, McCall K. Programmed cell death in the germline. Semin Cell Dev Biol 2005; 16:245–259.
8. Wang RA, Nakane PK, Koji T. Autonomous cell death of mouse male germ cells during fetal and postnatal period. Biol Reprod 1998; 58: 1250–1256.
9. Hamer G, Roepers-Gajadien HL, Gademan IS, Kal HB, De Rooij DG. Intercellular bridges and apoptosis in clones of male germ cells. Int J Androl 2003; 26:348–353.
10. Hochwagen A, Amon A. Checking your breaks: surveillance mechanisms of meiotic recombination. Curr Biol 2006; 16:R217–R228.
11. Roeder GS, Bailis JM. The pachytene checkpoint. Trends Genet 2000; 16:395–403.
12. Roeder GS. Meiotic chromosomes: it takes two to tango. Genes Dev 1997; 11:2600–2621.
13. Deng W, Lin H. miwi, A murine homolog of piwi, encodes a cytoplasmic protein essential for spermatogenesis.Dev Cell 2002; 2:819–830.
14. Kuramochi-Miyagawa S, Watanabe T, Gotoh K, Takamatsu K, Chuma S, Kojima-Kita K, Shiromoto Y, Asada N, Toyoda A, Fujiyama A, Totoki Y, Shibata T, et al. MVH in piRNA processing and gene silencing of retrotransposons. Genes Dev 2010; 24:887–892.
15. Papaioannou MD, Pitetti JL, Ro S, Park C, Aubry F, Schaad O, Vejnar CE, Kuhne F, Descombes P, Zdobnov EM, McManus MT, Guillou F, et al. Sertoli cell Dicer is essential for spermatogenesis in mice. Dev Biol 2009; 326:250–259.
16. Ma L, Buchold GM, Greenbaum MP, Roy A, Burns KH, Zhu H, Han DY, Harris RA, Coarfa C, Gunaratne PH, Yan W, Matzuk MM. GASZ is essential for male meiosis and suppression of retrotransposon expression in the male germline. PLoS Genet 2009; 5:e1000635.
17. Jang W, Hua A, Spilson SV, Miller W, Roe BA, Meisler MH. Comparative sequence of human and mouse BAC clones from the *mnd2* region of chromosome 2p13. Genome Res 1999; 9:53–61.
18. Castilla LH, Perrat P, Martinez NJ, Landrette SF, Keys R, Oikemus S, Flanegan J, Heilman S, Garrett L, Dutra A, Anderson S, Pihan GA, et al. Identification of genes that synergize with Cbfb-MYH11 in the pathogenesis of acute myeloid leukemia. Proc Natl Acad Sci U S A 2004; 101:4924–4929.
19. Arango NA, Huang TT, Fujino A, Pieretti-Vanmarcke R, Donahoe PK. Expression analysis and evolutionary conservation of the mouse germ cell-specific *D6Mm5e* gene. Dev Dyn 2006; 235:2613–2619.
20. Bellve AR, Cavicchia JC, Millette CF, O'Brien DA, Bhatnagar YM, Dym M. Spermatogenic cells of the prepuberal mouse. Isolation and morphological characterization. J Cell Biol 1977; 74:68–85.
21. McCarrey JR, Berg WM, Paragioudakis SJ, Zhang PL, Dilworth DD, Arnold BL, Rossi JJ. Differential transcription of *Pgk* genes during spermatogenesis in the mouse. Dev Biol 1992; 154:160–168.
22. Nord AS, Chang PJ, Conklin BR, Cox AV, Harper CA, Hicks GG, Huang CC, Johns SJ, Kawamoto M, Liu S, Meng EC, Morris JH, et al. The International Gene Trap Consortium Website: a portal to all publicly available gene trap cell lines in mouse. Nucleic Acids Res 2006; 34: D642–D648.
23. Nagy A, Gertsenstein M, Vintersten K, Behringer R. Staining whole mouse embryos for β-galactosidase (*lacZ*) activity. CSH Protoc 2007; 2007:pdb.prot4725. DOI 10.1101/pdb.prot4725.
24. Bellani MA, Romanienko PJ, Cairatti DA, Camerini-Otero RD. SPO11 is required for sex-body formation, and Spo11 heterozygosity rescues the prophase arrest of *Atm*$^{-/-}$ spermatocytes. J Cell Sci 2005; 118: 3233–3245.
25. Kogo H, Kowa-Sugiyama H, Yamada K, Bolor H, Tsutsumi M, Ohye T, Inagaki H, Taniguchi M, Toda T, Kurahashi H. Screening of genes involved in chromosome segregation during meiosis I: toward the identification of genes responsible for infertility in humans. J Hum Genet 2010; 55:293–299.
26. Wang N, Tilly JL. Epigenetic status determines germ cell meiotic commitment in embryonic and postnatal mammalian gonads. Cell Cycle 2010; 9:339–349.
27. Yoshida S, Sukeno M, Nakagawa T, Ohbo K, Nagamatsu G, Suda T, Nabeshima Y. The first round of mouse spermatogenesis is a distinctive program that lacks the self-renewing spermatogonia stage. Development 2006; 133:1495–1505.
28. Noce T, Okamoto-Ito S, Tsunekawa N. Vasa homolog genes in mammalian germ cell development. Cell Struct Funct 2001; 26:131–136.
29. Enders GC, May JJ II. Developmentally regulated expression of a mouse germ cell nuclear antigen examined from embryonic day 11 to adult in male and female mice. Dev Biol 1994; 163:331–340.
30. Matzuk MM, Lamb DJ. The biology of infertility: research advances and clinical challenges. Nat Med 2008; 14:1197–1213.
31. Burgoyne PS, Mahadevaiah SK, Turner JM. The consequences of asynapsis for mammalian meiosis. Nat Rev Genet 2009; 10:207–216.
32. Mahadevaiah SK, Turner JM, Baudat F, Rogakou EP, de Boer P, Blanco-Rodriguez J, Jasin M, Keeney S, Bonner WM, Burgoyne PS. Recombinational DNA double-strand breaks in mice precede synapsis. Nat Genet 2001; 27:271–276.
33. de Vries FA, de Boer E, van den Bosch M, Baarends WM, Ooms M, Yuan L, Liu JG, van Zeeland AA, Heyting C, Pastink A. Mouse *Sycp1* functions in synaptonemal complex assembly, meiotic recombination, and XY body formation. Genes Dev 2005; 19:1376–1389.
34. Bolcun-Filas E, Hall E, Speed R, Taggart M, Grey C, de Massy B, Benavente R, Cooke HJ. Mutation of the mouse Syce1 gene disrupts synapsis and suggests a link between synaptonemal complex structural components and DNA repair. PLoS Genet 2009; 5:e1000393.
35. Okada Y, Scott G, Ray MK, Mishina Y, Zhang Y. Histone demethylase JHDM2A is critical for *Tnp1* and *Prm1* transcription and spermatogenesis. Nature 2007; 450:119–123.
36. Hasthorpe S, Tainton K, Peart M, Roeszler KN, Bell KM, Lusby PE, Hutson JM, Tymms MJ. G_2/M checkpoint gene expression in developing germ cells. Mol Reprod Dev 2007; 74:531–538.
37. Sun F, Handel MA. Regulation of the meiotic prophase I to metaphase I transition in mouse spermatocytes. Chromosoma 2008; 117:471–485.
38. Baudat F, Keeney S. Meiotic recombination: making and breaking go hand in hand. Curr Biol 2001; 11:R45–R48.
39. Ward JO, Reinholdt LG, Motley WW, Niswander LM, Deacon DC, Griffin LB, Langlais KK, Backus VL, Schimenti KJ, O'Brien MJ, Eppig JJ, Schimenti JC. Mutation in mouse *Hei10*, an E3 ubiquitin ligase, disrupts meiotic crossing over. PLoS Genet 2007; 3:e139.
40. Meng X, Akutsu H, Schoene K, Reifsteck C, Fox EP, Olson S, Sariola H, Yanagimachi R, Baetscher M. Transgene insertion induced dominant

male sterility and rescue of male fertility using round spermatid injection. Biol Reprod 2002; 66:726–734.
41. Eaker S, Pyle A, Cobb J, Handel MA. Evidence for meiotic spindle checkpoint from analysis of spermatocytes from Robertsonian-chromosome heterozygous mice. J Cell Sci 2001; 114:2953–2965.
42. Eaker S, Cobb J, Pyle A, Handel MA. Meiotic prophase abnormalities and metaphase cell death in MLH1-deficient mouse spermatocytes: insights into regulation of spermatogenic progress. Dev Biol 2002; 249: 85–95.
43. Odorisio T, Rodriguez TA, Evans EP, Clarke AR, Burgoyne PS. The meiotic checkpoint monitoring synapsis eliminates spermatocytes via p53-independent apoptosis. Nat Genet 1998; 18:257–261.
44. Lacefield S, Murray AW. The spindle checkpoint rescues the meiotic segregation of chromosomes whose crossovers are far from the centromere. Nat Genet 2007; 39:1273–1277.
45. Hassold TJ. The origin of aneuploidy in humans. Basic Life Sci 1985; 36:103–115.
46. Royo H, Polikiewicz G, Mahadevaiah SK, Prosser H, Mitchell M, Bradley A, de Rooij DG, Burgoyne PS, Turner JM. Evidence that meiotic sex chromosome inactivation is essential for male fertility. Curr Biol 2010; 20:2117–2123.
47. Vernet N, Mahadevaiah SK, Ojarikre OA, Longepied G, Prosser HM, Bradley A, Mitchell MJ, Burgoyne PS. The Y-encoded gene *Zfy2* acts to remove cells with unpaired chromosomes at the first meiotic metaphase in male mice. Curr Biol 2011; 21:787–793.